Journal of Materials Chemistry B

Accepted Manuscript

Journal Name

Journal of Materials Chemistry B

Dynamic Article Links ►

Cite this: DOI: 10.1039/c0xx00000x

www.rsc.org/xxxxxx

ARTICLE TYPE

Carbon dots from PEG for high sensitive detection of levodopa

Hao Li, Juan Liu, Sijie Guo,Yalin Zhang, Hui Huang,* Yang Liu and Zhenhui Kang

Received (in XXX, XXX) Xth XXXXXXXXX 20XX, Accepted Xth XXXXXXXXX 20XX
DOI: 10.1039/b000000x

A high-intensity fluorescence carbon dots (CDs) coupled with tyrosinase (TYR) obtained the hybrids, as fluorescence probe, which exhibit efficient, fast, stable and sensitive in the detection of levodopa (L-DOPA). The detection limit of L-DOPA is as low as $9.0*10^{-8}$ mol L^{-1} with a wide linear range from $3.17*10^{-4}$ mol L^{-1} to $3.11*10^{-7}$ mol L^{-1}. The efficient selective detection of L-DOPA can be attribute to the CDs are excellent electron acceptors/donors and available absorption capacity of H^+. It is worth mentioning that the TYR does not demand modification and immobilization, and the test results can be read as soon as the probe-sample incubation was completed. Moreover, the test results are comparable to that of the present clinical fluorescence and high performance liquid chromatography (HPLC). Our experiment results indicated the CDs possess great potential in the development of various enzyme-based biosensors.

Keywords: carbon dots, tyrosinase, levodopa, fluorescence probe, high sensitive detection

.

1. Introduction

Levodopa [L-3,4-dihydroxyphenylalanine (L-DOPA)], as the precursor of the neurotransmitter dopamine, is the most widely prescribed drug in the treatment of Parkinson's disease caused by the lack of dopamine. As a drug used in the clinical treatment of Parkinson's disease and levodopa-responsive dystonia, too much L-DOPA has many side effects, such as nausea, vomit, loss of appetite, insomnia, hallucinations, and other adverse reactions. Therefore, the efficient and sensitive detection of L-DOPA is an important feature in pharmaceutical and clinical procedures.[1] To date, many literatures have reported technique methods for analysis of L-DOPA concentration, such as high performance liquid chromatography (HPLC),[2] flow injection system,[3] spectrophotometric[4] and capillary zone electrophoresis with electrochemical detection.[5] Despite tremendous efforts being made to detection of L-DOPA, these methods still involved the use of organic solvents, long analysis time, complicated pretreatment techniques and expensive instruments. In recent years, many novel methods emerged for the detection of L-DOPA, such as electrochemical detection[6] and semiconductor QDs fluorescent probes.[7] However, seeking a simple, efficient and selective method to detect L-DOPA is still a great challenge.

The fluorescence carbon dots (CDs), as a new class of zero-dimensional carbon nanostructures, have attracted considerable interest in recent years, which are stable, low toxic, biocompatible and easy to functionalization and have strong and tunable photoluminescence (PL).[8~13] To date, there is a lot of reports revealed the CDs could be excellent candidates for biological sensors. However, there were few studies on the selective detection of L-DOPA with CDs as a high sensitive and stable fluorescent biosensor. Compared to other choices, the florescence method in detection of the L-DOPA is fast, efficient and sensitive. In view of the excellent fluorescence properties, the fluorescence CDs may become one of the most potential biosensors in the detection of L-DOPA.

Herein, we found a kind of CDs which possess high fluorescence quantum yields, excellent electron acceptors/donors and available absorption capacity of H^+ than any other CDs. The high-intensity fluorescence CDs coupled with tyrosinase (TYR) to obtain hybrids as fluorescence biosensor exhibit efficient, fast, stable and sensitive in the detection of L-DOPA. The detection limit of L-DOPA is as low as $9.0*10^{-8}$ mol L^{-1}, and the detection range is very wide from $3.17*10^{-4}$ mol L^{-1} to $3.11*10^{-7}$ mol L^{-1}. The efficient selective detection of L-DOPA can be attribute to the CDs are excellent electron acceptors/donors and available absorption capacity of H^+. It is worth mentioning that the TYR does not demand modification and immobilization, and the test results can be read as soon as the probe-sample incubation was completed. More important, the test results are comparable to that of the present clinical method (HPLC method).

2. Experimental Section

2.1 Instruments and Chemicals.

Transmission electron microscopy (TEM) and high-resolution TEM (HRTEM) images were carried out using a FEI/Philips Tecnai G2 F20 TWIN transmission electron microscope at an acceleration voltage of 200 kV. The UV-vis spectra were measured with an Agilent 8453 UV-Vis Diode Array Spectra photometer, while the photoluminescence (PL) study was conducted with a Horiba Jobin Yvon (Fluoro Max-4) Luminescence Spectrometer. The fluorescence quantum yield was performed on a Fluorolog-TCSPC Luminescence Spectrometer. The Fourier Transform Infrared (FTIR) spectra of CDs were obtained with a Varian Spectrum GX spectrometer. The human urine samples were detected by the HP Agilent 1100 Series HPLC. In our work, we didn't involve the use of live animals. Human blood samples were provided by the Hospital of Jilin University and all experiments were performed in compliance with the relevant laws and institutional guidelines.

Levodopa and TYR (845U/mg) were purchased from USA Worthington Biochemical Co. Ltd. Carbon rods (diameter of 5 mm) were purchased from Shanghai Moyang electronic and carbon Co. Ltd. (Shanghai, China). Anhydrous ethanol (analytical grade), polyethylene glycol (PEG 200, PEG 600 and PEG 800), 2, 4-dinitrotoluene and N, N-diethylaniline were purchased from Adamas-beta. All other chemicals used in this work were of analytical grade. Except the specific statement, the detection buffer was PB buffer (pH=6.8, 0.05 M sodium phosphate). Milli-Q ultrapure water (Millipore, ⩾ 18 MΩ cm) was used throughout.

2.2 Preparation of CDs by Electrolytic Method with PEG as Carbon Sources (CDs1, CDs2 and CDs3).

To avoid confusion, the different CDs from different carbon sources were defined as CDs1 from PEG 200, CDs2 from PEG 600 and CDs3 from PEG 800. In a typical experiment, 3.0 g NaOH was added to a mixed solution of 50 mL PEG 200 and 10 mL distilled water to form a clear solution. Then the mixed solution would become brown after electrolysis for 6 h. To remove the impurities, the raw solution was given a dialysis treatment using a semi-permeable membrane (MWCO 1000). At last, the obtained solution was changed to golden yellow, implying we got the CDs1. For the preparation of CDs2 and CDs3, the PFG 200 was respectively substituted by PEG 600 and PEG 800 during the same synthesis process.

2.3 Preparation of CDs by Reflux Method with Glucose as Carbon Sources (CDs4 and CDs5).

1.5 g glucose was dissolved in the 5 mL distill1ed water to form a clear solution. Then 3 mL HCl (or HNO_3) was added into the above solution. Afterwards, the mixture was heated at 90 ℃ for 6 h under reflux and then given a dialysis treatment using a semi-permeable membrane (MWCO 3000) to remove the impurities. After filter, the obtained solution was brown, implying the formation of CDs4 (or CDs5).

2.4 Preparation of CDs by Ultrasonic Method with Glucose as Carbon Sources (CDs6).

A suitable amount of glucose was dissolved in deionized water (50 mL) to form a clear solution (1 mol/L). NaOH (50 mL, 1 mol/L) solution was added into the above solution, and the mixed solution was treated ultrasonically for 4 h. The final brown solution was given a dialysis treatment using a semi-permeable membrane (MWCO 3000) to remove the impurities. After that, the CDs6 could be obtained.

2.5 Analytes Sensing by PL Detection.

For all experiences, the texts were repeated at least three times to ensure the accuracy of the measurements. All of the PL spectra were recorded on the same fluorescence spectrophotometer. The fixed excitation wavelength of 370 nm was employed with a scan rate of 5 nm/s. 500 µL CDs2 solution was mixed with 20 mL (0.02 mg/mL) TRY solution. The L-DOPA solutions with different concentrations were added into 2 mL TRY/CDs hybrid. After that, the mixed solution was diluted to 4 mL with PB, which was incubated at 35 ℃ for 35 min. At last, the mixture was measured by PL Spectrometer. All kinds of CDs were used for detection of L-DOPA.

2.6 Adsorption Equilibrium Measurements.

The following experiments were tested in the water solution. In order to study the proton (H^+) adsorption capacity of CDs, 0.005 M HCl solution was selected to investigate the adsorption behaviour of CDs. Due to the excellent water solubility of CDs, the adsorption experiments were conducted with a dialysis method.[14] The CDs solution was dialyzed using a semi-permeable membrane (MWCO 1000) in a 600 mL beaker, and the dialysate was 0.005 M HCl (500 mL). Notably, the CDs were treated by dialysis method before using, so CDs would not dialyze out of semi-permeable membrane. If CDs have good adsorption behaviour of H^+, H^+ would gradually cross semi-permeable membrane and dialyze into CDs solution. After stirring on a shaker for predetermined time intervals, the residual concentration of HCl solution was determined by titrating with 0.005 M NaOH solution.

2.7 SDS-Polyacrylamide Gel Electrophoresis (SDS-PAGE).

TYR/CDs2 hybrids and CDs2 were loaded onto SDS polyacrylamide gels (20%) respectively and electrophoresed at 50 mA under the air atmosphere. Imaging of gels was carried out by UV illumination and visible light.

3. Results and Discussion

3.1 The Structures and PL Properties of CDs1~3.

The morphology and optical properties of CDs2 are shown in Fig. 1, while the TEM images of CDs1, CDs3, CDs4, CDs5 and CDs6 are shown in Fig. S1a, Fig. S2a, Fig. S3, Fig. S4 and Fig. S5, respectively. These images revealed that the obtained CDs are approximately 4.5~7 nm and well dispersed with each other, which are consistent with the DLS data as shown in Figure S17. The digital photos of CDs2 in aqueous solution under visible and UV (at 365 nm excitation) lights are shown inset in Fig. 1a, respectively, and the green fluorescent colour of CDs2 is easily observed by the naked eyes. The black line in Fig. 1b demonstrates the UV-vis absorption spectrum of CDs2, which shows the CDs possess an absorption peak in the range from 251 nm to 270 nm. The absorption band represents the typical absorption of an aromatic π system, which is similar to that of polycyclic aromatic hydrocarbons.[15] The Fourier transform infrared (FTIR) spectroscopy was employed to identify the functional groups of the as-prepared CDs2 shown in Fig. 1b (red line). The peaks around 3400, 1640, and 1080 cm^{-1} are respectively corresponding with the vibrations of -OH, C=O, and C-O bonds, in which different bands deduce that the surface of the obtained CDs2 were occupied by hydrophilic groups (-OH and -COOH). These hydrophilic groups led to the good water dispersibility of CDs2, which greatly widen their further sensor application in aqueous system and the organisms system. The UV-vis absorption spectra and FTIR spectroscopy of CDs1 and CDs3 are similar to that of the spectra of CDs2 shown in Fig. S1b and Fig. S2b, respectively.

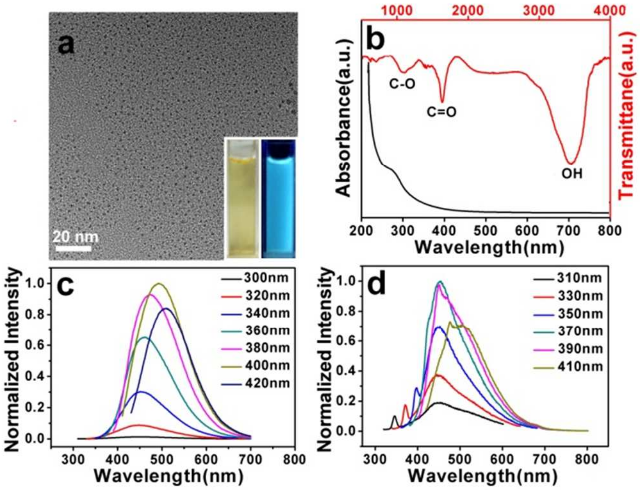

Figure 1. (a) Typical TEM image of CDs2, insets are the digital photos of CDs2 under visible and UV light (at 365 nm excitation). (b) UV-vis absorption and FTIR spectra of CDs2 (black and red lines, respectively). (c) and (d) PL spectra of CDs2 with different excitation wavelengths in the water and PB (pH=6.8), respectively.

Fig. 1c shows the PL spectra of CDs2 with different excitation wavelengths in the aqueous solution. With increase the excitation wavelength from 300 nm to 420 nm, the emission peaks gradually shifted to higher wavelengths accompanied with increased fluorescence intensity, among which the optimal excitation wavelength was 400 nm with the strongest emission peak at 485 nm. This bath chromic shift of emission from CDs2 has also been reported previously.[16~19] In the followed PL tests, the detailed PL spectra of CDs2 in PB solution (pH=6.8) were also investigated with different excitation wavelengths. As shown in Fig. 1d, the optimal excitation wavelength was obtained at 370 nm with the strongest emission peak at 470 nm in PB solution. These results demonstrate that the CDs2 possess stable and strong fluorescence, which may serve as an excellent fluorescence probe for bio-detection. Moreover, the PL spectra of CDs1 and CDs3 with different excitation wavelengths in water and PB are shown in Fig. S1c, Fig. S1d, Fig. S2c and Fig. S2d, respectively, which could conclude the similar conclusions compared to CDs2.

In the followed experiments, the quantum yield of CDs was measured according to the established procedure by using quinine sulfate in 0.10 M H_2SO_4 solution as the standard. The absorbance was measured on a Perkin Elmer LS 55 Spectrophotometer. Absolute values are calculated according to the following equation:

$$Q = Q_R \frac{m}{m_R} \frac{n^2}{n_R^2} \quad (1)$$

Where, Q is the quantum yield, m is the slope of the plot of integrated fluorescence intensity vs absorbance and n is the refractive index (taken here as 1.33, the refractive index of distilled water). The subscript refers to the reference fluorophore, quinine sulphate solution. In order to minimize re-absorption effects, absorbance in the 1 cm quartz cuvette was kept below 0.15 at the excitation wavelength of 375 nm.[20] So the PL quantum yields of CDs2, CDs1 and CDs3 were about 38 %, 36 % and 32 %, respectively. Furthermore, as shown in Fig. S6, CDs2 possess the highest fluorescence intensity in the three kinds of CDs.

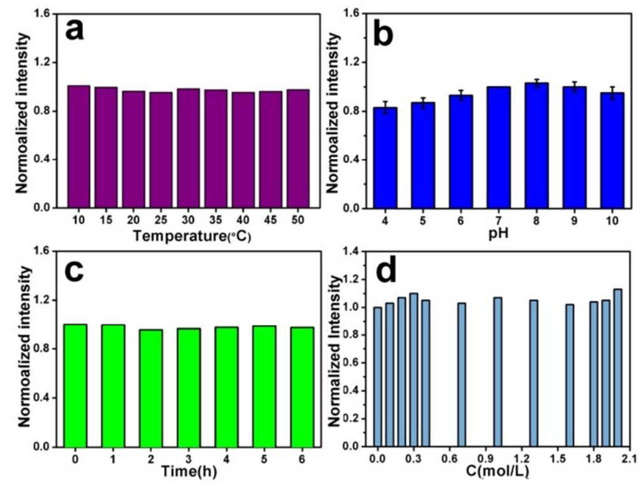

Figure 2. The effects of different temperatures (a), pH (b), stabilization time (c) and ionic strength in NaCl aqueous solution (d) on the normalized fluorescence intensity of CDs2 in PB solution.

To confirm the fluorescence stability of CDs2, the effects of different temperature, pH, stabilization time and ionic strength in NaCl aqueous solution on the PL intensity of CDs2 were tested in PB solution. Fig. 2a reveals the effect of different temperatures on the normalized fluorescence intensity of CDs2 in PB solution. As shown, when the temperature increased from 10 ℃ to 50 ℃, the PL intensity of CDs2 was almost the same, which indicated that the temperature did not affect the PL intensity of CDs2. Using the fluorescence intensity of CDs (pH=7.0) as a standard, as shown in Fig. 2b, when the pH of solution was changed from 4.0 to 8.0, the fluorescence intensity increased with pH firstly and subsequently decline, among which the CDs2 show the strongest PL emission intensity when the pH value was 8.0 (The fluorescence intensity increased 3 %). The results are similar to the physiological pH environment (pH= 7 ~ 8). Under strongly acidic (pH< 6.0) or alkaline conditions (pH> 9.0), the PL of CDs2 would be quenched and the fluorescence intensity decreased 17 % ~ 5 %. In addition, when the CDs2 were diluted by PB (pH 8.0), it retain excellent photo-stability over 6 h in air (Fig. 2c). Fig. 2d shows the influence of different ionic strength in NaCl aqueous solution on the PL intensity of CDs2. As shown, there was no obvious change on PL intensity even in aqueous solution with high ionic strength (2 M NaCl). All of above results revealed that the fluorescence of CDs2 are extremely stable under high temperature (50℃), acid or alkaline, strong ionic strength, which are profoundly suitable for practical biological detection. The fluorescence stability of CDs1 and CDs3 were also shown in Fig. S7 and Fig. S8, which display that their fluorescence stabilities were similar to that of CDs2.

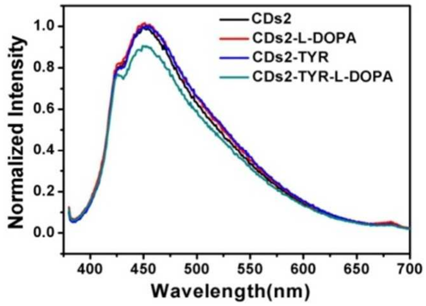

Figure 3. The fluorescence spectra of CDs2 (black line), CDs2 in the presence of 0.32 mM L-DOPA (CDs2-L-DOPA, red line), CDs2 in the presence of 20 μg mL^{-1} TYR (CDs2-TYR, blue line), and CDs2 in the presence of a mixture containing 20 μg mL^{-1} TYR and 0.32 mM L-DOPA (CDs2-TYR-L-DOPA, green line), respectively.

3.2 The Properties and characterization of the TYR/CDs hybrids.

In the followed experiments, to confirm the enzyme/carbon dots (TYR/CDs) hybrids as fluorescence biosensor can efficient in detection of L-DOPA and the feasibility of this method, a series experiments were carried out. Fig. 3 reveals the detailed PL comparisons using CDs2, CDs2 with L-DOPA, CDs2 with TYR and CDs2 with both TYR and L-DOPA. As shown, CDs2 exhibit obviously emission peak at approximately 455 nm (black line). When the L-DOPA was added in the solution including CDs2, the emission peak didn't show distinctly change under the same excitation wavelength (red line). The emission peak was also no change by addition of the TYR (blue line). However, both TYR and L-DOPA have been added in the solution containing CDs2, the emission peak reveals visibly quench (green line). In the whole process, the TYR can catalyze the L-DOPA to produce levodopachrome, which have a strong absorption at 490 nm. Therefore, the PL of CDs2 can efficient quench by in the solution with both TYR and L-DOPA. These results demonstrate that fluorescence CDs2 combined with TYR to form a fluorescence biosensor that can efficient in the detection of L-DOPA. The same experiments were also carried out with CDs1 and CDs3. As shown in Fig. S9 and Fig. S10, the TYR or L-DOPA is also unaffected the fluorescence of CDs1 and CDs3. But when the combinations TYR with L-DOPA were added in CDs (CDs1 or CDs3) solution, the fluorescence of CDs1 and CDs3 were quenched efficiently. So the CDs (CDs1 or CDs3) can also detect the L-DOPA effectively.

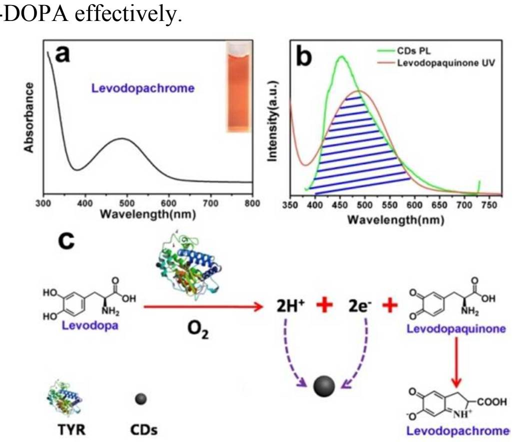

Figure 4. (a) UV-vis absorption spectrum of levodopachrome, inset is the corresponding digital photo under visible light. (b) Superposed graphs of levodopachrome UV spectrum and CDs PL spectrum. (c) Schematic illustration of the mechanism in the detection of L-DOPA.

Here, when the TYR was added in the L-DOPA solution, the mixture solution would become orange gradually in 30 min, in which the L-DOPA can be catalyzed to levodopaquinone by the TYR. The levodopachrome will be converted by a rapid spontaneous auto-oxidation to levodopachrome. And the levodopachrome has a large coverage from 400 nm to 600 nm shown in Fig. 4a. Fig. 4b reveals the superposed graphs of levodopachrome UV spectrum (green line) and CDs PL spectrum (red line), as shown, there is a large coverage from 400 nm to 600 nm,[21] indicating the levodopachrome is capable to quench the fluorescence of CDs2. According the above results, the possible mechanism in the detection of L-DOPA is concluded as follows: the TYR can catalyze the L-DOPA to form levodopachrome (2 mL of TYR (20 μg mL^{-1}) was added into 2 ml L-DOPA (0.13 mM) and left for 35 min at 35℃, pH= 6.8), which possesses a strong fluorescent absorption at 490 nm (pH= 6.8) and is capable to quench the fluorescence of CDs2. The L-DOPA was catalytically oxidized not only to produce levodopachrome, but also to produce the H^+ and e^-. If the produced H^+ and e^- were absorbed, the positive reaction would be promoted. In another words, that can shorten the reaction time (detection time). The CDs2, as excellent both electron acceptors and donors, and proton (H^+) adsorption capacity, can valid adsorption of H^+ and e^-, which could prompt the quenching process to achieve the efficient testing.[9] Therefore, based on the above, the TYR/CDs2 hybrids are efficient, stable, fast and sensitive fluorescence biosensor in the detection of L-DOPA. As a kind of high sensitive detection probe, it should have the following conditions: Firstly, the activity of enzyme should be higher. Secondly, the fluorescence intensity of probe should be stronger. Thirdly, the material should have the electron acceptors and donors' capacity and proton (H^+) adsorption capacity. Therefore, the TYR/CDs2 hybrids may be the optimal candidate in detection of L-DOPA.

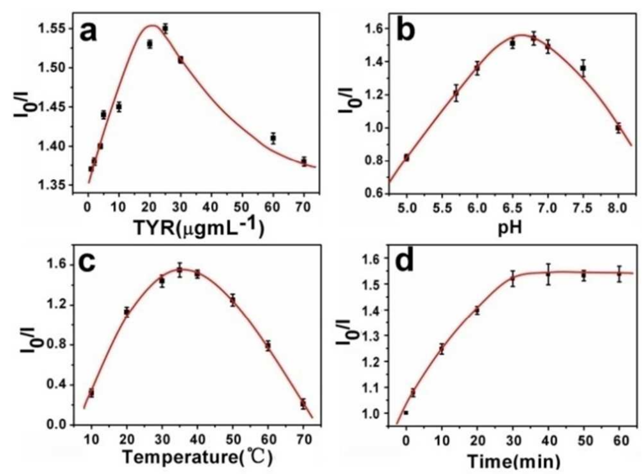

Figure 5. The effects of different TYR concentrations (a), pH (b), temperatures (c) and incubation times (d) on the quenched efficiency of the CDs2 in the presence of 0.13 mM L-DOPA and 20 μg mL^{-1} TYR solution (I_0 and I are CDs PL intensity in the absence and presence of analysts, respectively).

To obtain the optimal detection conditions, a series of control experiments (for the detection of L-DOPA) were carried out with different concentrations of TYR, different temperatures, pH values and incubation times. Fig. 5a shows when the concentration of CDs2 was constant (0.005 g/mL), the different concentrations of enzyme (TYR) effect on the detection of L-DOPA. As shown, with increase the concentration of TYR, the PL ratio increased at first then decreased. So the 20 μg mL^{-1} of TYR is optimal concentration. Fig. 5b reveals the influence of different pH values on the detection of L-DOPA. When the pH was changed from 5.0 to 8.0, the ratio I_0/I (I_0 and I are CDs PL intensity in the absence and presence of analysts, respectively) also increased firstly and then decreased after 6.8, and the optimum pH is 6.8. So the 6.8 was chosen as the favourable pH for the detection of L-DOPA. As shown in Fig. 5c, with the temperature increased from 10 ℃ to 70 ℃, the highest point of the ratio I_0/I had appeared at 35 ℃. So the 35 ℃ is the optimal incubated temperature. Fig. 5d reveals when the incubation time reached 35 min, the signal response sustained a stable value. Therefore, the optimal detection condition for L-DOPA is 35 ℃, pH=6.8 with the incubation time of 35 min. The same experiments are also carried out with CDs1 and CDs3. The optimal detection temperature and pH value for L-DOPA with CDs1 and CDs3 are 35 ℃, pH=6.8 (shown in Fig. S11b, Fig. S11c, S12b and S12c), but the incubation time is different. As shown in Fig. S11d and Fig. S12d, the incubation time of CDs1 and CDs3 are about 40 min and 50 min, respectively.

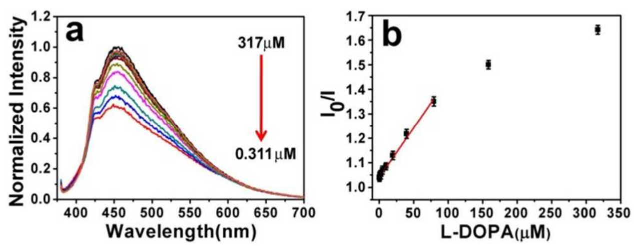

Figure 6. (a) The normalized fluorescence spectra of CDs2 containing 20 μg mL^{-1} TYR upon addition of different concentrations of L-DOPA from 317 μM to 0.311 μM. (b) The linear response of the quenching efficiency I_0/I of the CDs2 vs. concentrations of L-DOPA.

Based on the optimal conditions (at 35℃, pH=6.8 with the incubation time of 35 min), the selective detection of L-DOPA was explored. Fig. 6a shows the normalized PL spectra of CDs2, which were quenched in different concentrations of L-DOPA from 317 μM to 0.311 μM. The ratio I_0/I of normalized fluorescence intensity of CDs2 (I_0 and I are CDs PL intensity in the absence and presence of analysts, respectively) was proportional decrease to the different L-DOPA concentration, with the linear regression equation being $I_0/I=1.04+0.004C_{L\text{-}DOPA}$ (R^2=0.984, Fig. 6b). The detection limit of L-DOPA was tested at $9.0*10^{-8}$ mol L^{-1}. And the detection range is from $3.17*10^{-5}$ mol L^{-1} to $3.11*10^{-7}$ mol L^{-1}. However, at higher concentration, the quenching curve tends to be flat. This tendency is in accordance with the kinetics of enzyme-catalyzed reactions.[22, 23] The low detection limit and wide detection range proved that the CDs2 are efficient, stable, fast and sensitive fluorescence biosensor in the detection of L-DOPA. For CDs1 and CDs3, the experimental results also show that the detection range was the same as that of CDs2. (shown in Fig. S13 and Fig. S14). Due to their fluorescence intensities were different (shown in Fig S3), their low detection limit were different. The apparent low detection value of the CDs1 and the CDs3 were determined to be $6.2*10^{-8}$ mol L^{-1} and $7.0*10^{-8}$ mol L^{-1}, respectively.

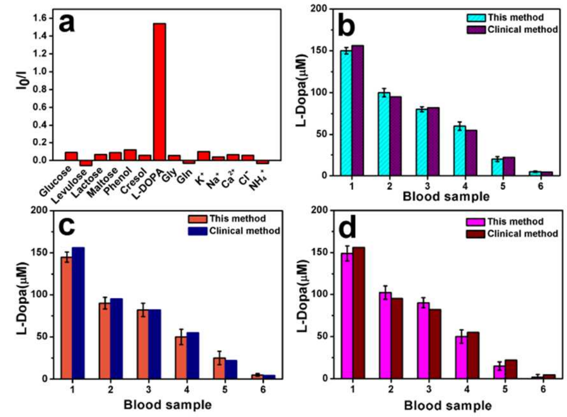

Figure 7. (a) The specificity effects of guest molecules (10 mM) to 0.13 mM L-DOPA on the PL of CDs2 containing 20 μg mL^{-1} TYR. The comparison with the fluorescence method and HPLC used TYR/CDs hybrids with different kinds of CDs: (b) CDs2, (c) CDs1, and (d) CDs3.

To further prove the specificity of developed fluorescence biosensor for L-DOPA, different guest molecules were chosen to detect, such as, metal ions, amino acids, phenol and cresol. As shown in Fig. 7a, TYR/CDs2 hybrids reveal the obvious specificity in detection of L-DOPA rather than those of the phenol, cresol, amino acids and metal ions, indicating the CDs2 can selective detection of L-DOPA.

In order to evaluate the applicability of the proposed method, the sensor system has been applied for L-DOPA analysis in biological assays. Notably, this detection method based on CDs2 can be directly used in real situation for its high sensitivity and selectivity. Six human blood samples were employed to detect L-DOPA by the developed method (TYR/CDs2), which were provided by the Hospital of Jilin University. All measurements were performed in PB, pH=6.8, incubated at 35 ℃ for 35 min. Before use, the blood sample was clotting in N_2 atmosphere. After clotting, the blood samples were centrifuged at 3000 rpm for 20 min. The supernatants were used as the serum samples. To minimize metal contamination, poly (propylene) syringes and silicone-coated glass tubes were soaked in 2 M HCl for 2 d, rinsed with pure water and dried. All the solutions were stored at 4℃. Samples 1~6 are the six different human blood samples with different L-DOPA concentration. The same six human blood samples were also detected by HPLC method. As shown in Fig. 7b, these results obtained by the two methods were matched well, which revealed the simple, fast and inexpensive fluorescence method based on TYR/CDs can be successfully applied in detecting L-DOPA with blood samples. We also use the other two kinds of CDs (CDs1 and CDs3) to test the same six human blood samples. As shown in Fig. 7c and Fig. 7d, these test data reveal that the other two kinds of CDs to combined with the TYR as fluorescent biosensor to detect L-DOPA are relatively inefficient, and their relative errors (test paper detection vs. HPLC clinical detection) are all larger than that of CDs2, as shown in the Table S1. Table S1 presents a comparison between HPLC method and fluorescence method for the values of six human blood samples. The calculation results reveal that the fluorescence method for determination of L-DOPA in this paper is rapid, precise and of low cost and it may be suitable for routine analysis. Why the CDs2 was the optimal candidate for fluorescent biosensor? That may attribute to the electron acceptor/donor properties and absorbing H^+ property of CDs2 were the strongest in the three kinds of CDs (CDs1, CDs2 and CDs3) and the PL quantum yields of CDs2 was the highest. Therefore, the CDs2 were the optimal candidate for fluorescent biosensor in the three kinds of CDs. We can conclude that if the PL quantum yield of CDs2 increase, the lower detection limit and broader detection range will expand. We can also design the novel biosensor based on the assembly of CDs2 with redox enzymes to detect other bio-molecules and medicament.

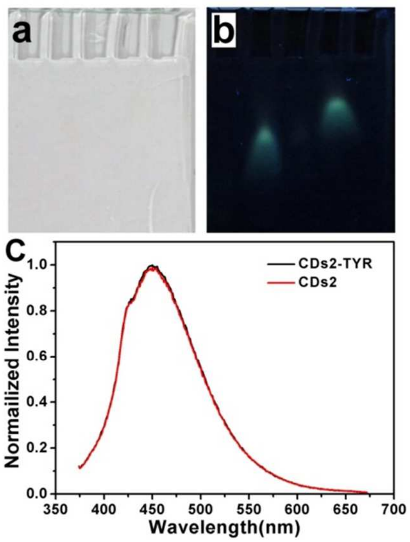

Figure 8. SDS-PAGE of the CDs2 (the second lane in Figure 8a) and TYR/CDs2 hybrids (the fourth lane in Figure 8a) used to separate mixtures on 20% gels. Gels were photographed under (a) visible light and (b) UV illumination. (c) The PL spectra of TYR/CDs2 (black trace) and CDs2 (red trace) in the PB solution, respectively.

To further probe the interaction between CDs2 and TYR in the hybrids, CDs2 and TYR/CDs2 hybrids were separated respectively by SDS-PAGE (sodium dodecyl sulfate polyacrylamide gel electrophoresis). Fig. 8a shows the complexes did not stain the SDS-PAG Egels under visible light because CDs2 and TYR/CDs2 are colourless (the second lane and the fourth lane in Fig. 8a, respectively). Fig. 8b reveals the stable complexes can be formed with CDs2 and TYR, which showed that CDs2 are moving faster than TYR/CDs2 hybrids (the second lane and the fourth lane in Fig. 8b, respectively). This effect may due to an increase in the hydrodynamic radius of the CDs2 upon adsorption of the PPL.As shown in Fig. 8c, the PL spectrum of CDs2 (red trace) was similar with the PL spectrum of the TYR/CDs2 hybrids (black trace), which indicated CDs2 are connected to the TYR by non-covalent bonds.

3.3 The Electron Acceptors and Donors Capacity of CDs.

To investigate the light-induced electron transfer properties of the CDs2, the time-correlated single-photon counting (TCSPC) experiments were performed. As shown in Fig. 9a and 9b, CDs2 exhibit a broad luminescence peak at about 550 nm with the excitation at 485 nm, and the emission intensities can be quenched by the known electron acceptors 2, 4-dinitrotoluene (-0.9 V vs. NHE)[24] and electron donors N, N-diethylaniline (DEA, 0.88 V vs. NHE).[25] Fig. 9c and 9d show the luminescence decays (485nm excitation, monitored with a 550 nm narrow band pass filter) of CDs2, with the observed Stern–Volmer (insets of Fig. 9c and 9d) quenching constants (K_{SV}=τF°kq) from linear regression of 32.0 M^{-1} and 22.0 M^{-1}, respectively. The above results demonstrate that the PL of CDs2 can be quenched highly efficiently by either electron acceptors or electron donors clearly confirm that CDs2 are excellent as both electron acceptors and electron donors.

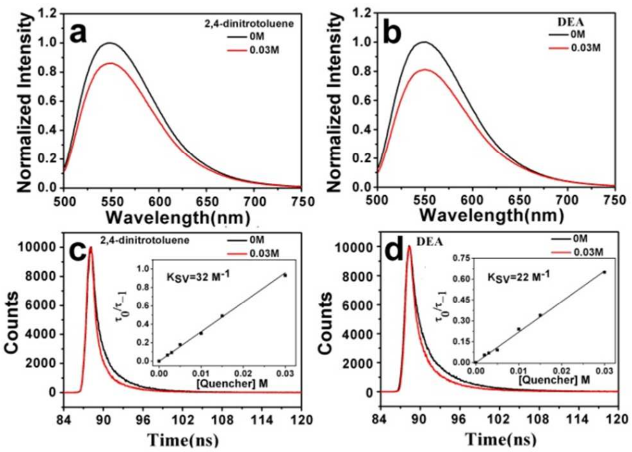

Figure 9. (a) and (b) Luminescence spectra of the CDs2 in toluene without and with the quenchers (2, 4-dinitrotoluene and DEA, both 0.03 M). (c) and (d) Luminescence decays (485 nm excitation, monitored with 550 nm narrow band pass filter) of the CDs2 with 2, 4-dinitrotoluene and DEA, respectively. Inset: Stern–Volmer plots for the quenching of luminescence quantum yields (485 nm excitation) of the CDs2 by(c) 2, 4-dinitrotoluene and (d) DEA.

To further establish the electron transfer properties of CDs can affect the detection of L-DOPA, the electron transfer properties of CDs1 and CDs3 were carried out for comparison with CDs2. Fig. S15 and S16 show the TCSPC experiments with CDs1 and CDs3. As shown, the quenching constants (K_{SV}=τF°kq) of CDs1 are about 20 M^{-1} for K_1 and 18 M^{-1} for K_2 under visible light (K_1 for electron acceptor, 2, 4-dinitrotoluene; K_2 for electron donor, DEA), while the quenching constants of CDs3 are 18 M^{-1} for K_1 and 15 M^{-1} for K_2. Obviously, the quenching constants for CDs2 (32.0 M^{-1}) are larger than that of the CDs1 and CDs3. The results reveal the CDs2 are highly efficient electron donors, which can better absorb the e^- and promote the catalytic reaction.

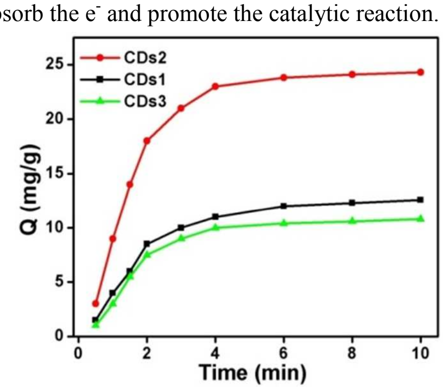

Figure 10. Dependence of contact time on removal of H^+ by different CDs (CDs1 (black line), CDs2 (red line) and CDs3 (green line), respectively).

3.4 The Proton (H^+) Adsorption Capacity of CDs.

To testify the proton (H^+) adsorption capacity of CDs can affect the detection of L-DOPA, the proton adsorption experiments with different CDs (CDs1, CDs2 and CDs3) were investigated in the (0.005 M) HCl solution. Due to the CDs are full of functional groups, such as -OH, -COOH and -C=O on the surface, the uncontrolled hydrophilic groups of CDs may help to draw the H^+ closer to the surface of CDs, which are good for enhancing the adsorption capacity.[26, 27] On account of the excellent water solubility of CDs, the adsorption experiments were conducted with a dialysis method (see Experimental section for details). The amount of adsorbed HCl, Q (mg/g) was calculated by the following equation:

$$Q=\frac{(C_0\text{-}C_e)\cdot V}{1000W}\ (2)$$

Where C_0 and C_e are the initial and equilibrium concentration (mg/L), respectively, V is the volume of HCl solution (mL) and W is the weight (g) of CDs adsorbent. The adsorption behavior of CDs was conducted at the same condition, and the concentration and volume of CDs solution were same. Fig. 10 shows the dependence of contact time on removal of H^+ by different CDs (CDs1 (black line), CDs2 (red line) and CDs3 (green line), respectively), from which the adsorption of H^+ was extraordinary rapid in the first 4 min, then gradually increased as the prolongation of contact time. After 6 min of adsorption, the amount of H^+ remains constant, which suggests that 6 min is the equilibrium time in this adsorption experiments. And the amount of adsorbed H^+ (based on the quality of HCl) was about 12.6 mg/g, 24.6 mg/g and 10.9 mg/g for CDs1, CDs2 and CDs3 respectively. These results indicated the CDs2 possess better absorption capacity of H^+, and the Fig. 5d, Fig. S8d and Fig. S9d reveals that the incubation time of CDs2 were the shortest, which could promote the sensitive detection of L-DOPA.

In the following experiments, the equilibrium of sorption was further evaluated by two well-known models of Langmuir and Freundlich isotherm. The Langmuir isotherm is the most extensively used two-parameter equation, which assumes monolayer adsorption onto the surface containing a limited number of adsorption sites with no transmigration of the adsorbate in the plane of the surface.[28] It generally expresses in the following equation:

$$\frac{C_e}{Q_e}=\frac{1}{Q_m K_L}+\frac{1}{Q_m}C_e\ (3)$$

Where C_e is the equilibrium adsorbated concentration (mg/L), Q_e is the amount of adsorbate adsorbed per mass unit of adsorbent at equilibrium (mg/g), Q_m is the maximum mass adsorbed at saturation conditions per mass unit of adsorbent (mg/g), and K_L is the empirical constant with units of inverse of concentration C_e (L/mg). The fundamental characteristic of Langmuir equation can be expressed in terms of a dimensionless separation factor R_L, which is defined as:

$$R_L=\frac{1}{1+K_L C_0}\ (4)$$

Where K_L is the Langmuir isotherm constant (L/mg) and C_0 is the initial HCl concentration (mg/L). The R_L value indicates the type of the isotherm to be either favourable ($0<R_L<1$), unfavourable ($R_L>1$), linear ($R_L=1$) or irreversible ($R_L=0$).

The Freundlich isotherm in the other hand takes heterogeneous systems into account and is not restricted to the formation of the monolayer.[29] The well-known logarithmic form of the Freundlich isotherm is given by the following equation:

$$InQ_e=InK_F+\left(\frac{1}{n}\right)InC_e\ (5)$$

As a Freundlich constant, here K_F (mg/g) can be defined as an adsorption or distribution coefficient and represents the amount of adsorbed on an adsorbent for a unit equilibrium concentration. While n is an indication of how favourable the adsorption process. The slope of 1/n ranging between 0 and 1 is a measure of adsorption intensity or surface heterogeneity, becoming more heterogeneous as its value gets closer to zero. A value for 1/n below 1 indicates a normal Langmuir isotherm while 1/n above 1 is indicative of cooperative adsorption.[30]

Table 1. Langmuir and Freundrich isotherm constants for H^+ onto different CDs (CDs1, CDs2 and CDs3, respectively).

	Langmuir				Freundlich		
	Q_m	K_L	R_L	R^2	K_F	1/n	R^2
CDs2	24.6	0.043	0.652-0.115	0.998	2.02	0.558	0.996
CDs1	12.6	0.086	0.48-0.060	0.995	1.63	0.576	0.974
CDs3	10.9	0.10	0.441-0.052	0.999	1.21	0.629	0.997

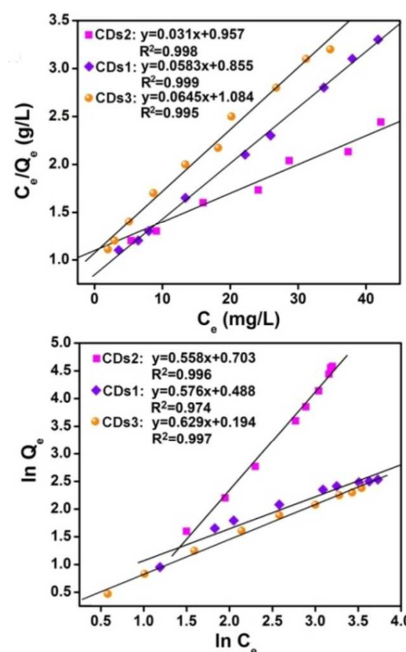

Figure 11. (a) Langmuir isotherm for adsorption of H^+ by different CDs and. (b) Freundlich isotherm for adsorption of H^+ by different CDs.

Fig. 11a and 11b show Langmuir and Freundlich isotherms for different CDs (CDs1, CDs2 and CDs3, respectively). Isotherm parameters and the correlation coefficients, R_2, were calculated and summarized in Table 1. As shown in the Table 1, the Langmuir isotherms for CDs2, CDs1 and CDs3 respectively with different correlation coefficients of 0.998, 0.995 and 0.999 represent a better fit of experimental data than Freundlich model with correlation coefficients of 0.996, 0.974 and 0.997, which indicate that monolayer adsorption of H^+ takes place on the homogeneous surface of CDs adsorbents. Moreover, the values of the dimensionless constants R_L for different CDs (CDs2, CDs1 and CDs3) are 0.652~0.115, 0.48~0.060 and 0.441~0.052, respectively, which suggest that the adsorption is favourable and rather irreversible. As showed in Table 1, the value of 1/n was between 0 and 1 for both adsorbents, which further proved the equilibrium of sorption for adsorption capacity of H^+ is suitable for Langmuir isotherm model.

In the next experiments, to evaluate adsorption kinetics, two common models were applied to the experimental data obtained at adsorption processes. These are pseudo-first-order and pseudo-second-order[31] kinetic models as shown in Eqs. (6) and (7), respectively:

$$ln(Q_e - Q_t) = lnQ_e - k_{pf}t \quad (6)$$

$$\frac{t}{Q_t} = \frac{1}{k_{ps}{Q_e}^2} + \frac{1}{Q_e}t \quad (7)$$

Where k_{pf} (min^{-1}) and k_{ps} (g/mol min) are the adsorption rate constant of pseudo first and second-order adsorptions, respectively; Q_e and Q_t are the amounts of dyes adsorbed at equilibrium and time t (mg/g) respectively.

Table 2. Pseudo-first-order and Peseudo-second-order models constants for the adsorption of H^+ on different CDs (CDs1, CDs2 and CDs3, respectively).

	Pseudo-first-order			Pseudo-second-order		
	Q_e	K_{pf}(min^{-1})	R^2	Q_e	K_{ps}(g/mol min)	R^2
CDs2	24.3	0.587	0.977	24.3	0.022	0.952
CDs1	12.6	0.484	0.995	12.6	0.034	0.962
CDs3	10.8	0.537	0.985	10.8	0.036	0.900

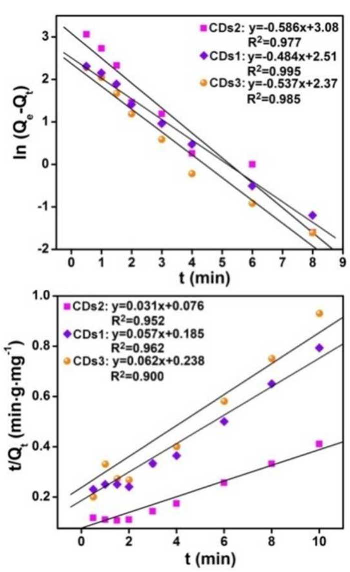

Figure 12. (a) Pseudo-first-order and (b) Pseudo-second-order kinetic models for adsorption of H^+ on different CDs (CDs1, CDs2 and CDs3, respectively).

The adsorption kinetic plots are shown in Fig. 12 and all the kinetic parameters determined are listed in Table 2. Since calculated correlation coefficients are closer to unity for pseudo-first-order kinetics model than the pseudo-second-order kinetic model (0.977, 0.995 and 0.985 vs. 0.952, 0.962 and 0.900 for different CDs, respectively), the present sorption systems follow predominantly the first-order rate model.

Table 3. The electron acceptor/donor properties and absorbed H^+ properties of different methods of as-synthesized CDs (CDs2, CDs4, CDs5 and CDs6, respectively).

CDs Species	K_1 (K_1 for electron acceptor)	K_2 (K_2 for electron donor)	Q (mg/g)
CDs2	32	22	24.6
CDs4	25	18	11
CDs5	24	19	10
CDs6	30	17	8

In order to find the best CDs as candidate for fluorescent biosensor, the electron acceptor/donor properties of different CDs have be performed, as shown in the Table 3. The quenching constants (K_{SV}=τF°kq) of CDs4 are about 25 M^{-1} and 18 M^{-1} (under visible light; K_1 for electron acceptor, 2, 4-dinitrotoluene; K_2 for electron donor, DEA). For theCDs5, the K_1 and K_2 are 24 M^{-1} and 19 M^{-1}, respectively. While the CDs6, the K_1 and K_2 are 30 M^{-1} and 17 M^{-1}, respectively. As shown, the CDs2 possess largest quenching constants (32.0 M^{-1} and 22.0 M^{-1}) than that of others (CDs1, CDs3, CDs4, CDs5 and CDs6), which reveal that the CDs2 show the strongest the electron acceptor/donor properties than that of others CDs. To further probe the strongest absorbing H^+ property of CDs, the adsorption experiments with different CDs were investigated. In the Table 3, after 1h of adsorption, the amount of adsorbed H^+ was about 24.6 mg/g, 11 mg/g, 10 mg/g and 8 mg/g for different CDs, respectively. These experimental data show that the adsorbed H^+ property of CDs2 was the strongest. Based on the above experimental data, these results indicate the CDs2 show the strongest electron acceptor/donor properties and adsorbed H^+ property, which were the optimal candidate for fluorescent biosensor. It not only plays the role of fluorescent indicator, but also promotes the catalytic reaction process.

4. Conclusions

We have developed a low-cost electrolysis method to obtain high-intensity fluorescent CDs with PEG as carbon source. The different kinds of PEG (PEG 200, PEG 600 and PEG 800) were employed to achieve the high-intensity fluorescence, among which the CDs using PEG 600 (CDs2) as carbon source exhibit the highest intensity fluorescence with the quantum yields of 38%. With the high quantum yields, the CDs can be promising candidate in the applications of bio-imaging, bio-labeling and biosensors. The high-intensity fluorescence CDs2 combined with TYR to form a fluorescence biosensor that exhibits efficient, fast, stable and sensitive in the detection of L-DOPA. The TYR was chosen as a catalyst due to it could catalyze the L-DOPA to form levodopachrome, which possesses a strong fluorescent absorption at 470 nm or 480 nm and is capable to quench the fluorescence of CDs. In the detection of L-DOPA, the detection limit can be obtained at $9.0*10^{-8}$ mol L^{-1} with a linear range from $3.17*10^{-4}$ mol L^{-1} to $3.11*10^{-7}$ mol L^{-1}. It was found that the efficient selective detection of L-DOPA can be attribute to the CDs are excellent electron acceptors/donors and available absorption of H^{+}. The possible mechanism in the detection of L-DOPA can be described that the L-DOPA was catalytically oxidized by TYR to produce levodopachrome, H^{+} and e^{-}. The H^{+} and e^{-} can be absorbed by CDs2 and simultaneously the levodopachrome can quench the PL of CDs. It is worth to concern that the present fluorescence probe didn't demand enzyme modification and immobilization, and the test results can be read as soon as the probe-sample incubation is completed. In present system, the test results are comparable to that of the present HPLC method (clinical method). More important, the CDs offer great potential in the development of various enzyme-based biosensors and portable sensing devices.

Acknowledgment

This work was supported by Collaborative Innovation Center of Suzhou Nano Science and Technology, the National Basic Research Program of China (973 Program) (2012CB825803, 2013CB932702), the National Natural Science Foundation of China (51422207, 51132006, 21471106), the Specialized Research Fund for the Doctoral Program of Higher Education (20123201110018), a Suzhou Planning Project of Science and Technology (ZXG2012028), the Natural Science Foundation of Jiangsu Province of China (BK20140310), China Postdoctoral Science Foundation (2014M560445), and a project funded by the Priority Academic Program Development of Jiangsu Higher Education Institutions (PAPD).

Notes and references

Jiangsu Key Laboratory for Carbon-Based Functional Materials & Devices, Institute of Functional Nano & Soft Materials (FUNSOM), Soochow University, 199 Ren'ai Road, Suzhou, 215123, Jiangsu, PR China; E-mail: hhuang0618@suda.edu.cn

† TEM images; PL spectra; UV-visspectra; SEM images and so on. See DOI: 10.1039/b000000x/

1. J. M. Cedarbaum, R. Williamson, H. Kutt and J. Chromatogr, *Biomed. Appl.,* 1987, **415**, 393.
2. S. F. Li, H. L. Wu, Yu,Y. J. Y. N. Li, J. F. Nie, H. Y. Fu and R. Q Yu, *Talanta,* 2010, **81**, 805.
3. M. F. S. Teixeira, L. H. Marcolino-Junior, O. Fatibello-Filho, E. R. Dockal and M. F. Bergamini, *Sens. Actuators. B.,* 2007, **122**, 549.
4. J. Coello, S. Maspoch and N. Villegas, *Talanta,* 2000, **53**, 627.
5. S. Zhao, W. Bai, B. Wang and M. He, *Talanta,* 2007, **73**, 142.
6. Y. Xu, M. Wu, X. Z. Feng, X. B. Yin, X. W. He and Y. K. Zhang, *Chem. Eur. J.*, 2013, **19**, 6282.
7. M. Hu, H. L. Yu, F. D. Wei, G. H. Xu, J. Yang, Z. Cai and Q. Hu, *Spectrochimica Acta Part A*, 2012, **91** 130.
8. A. B. Bourlinos, A. Stassinopoulos, D. Anglos, R. Zboril, M. Karakassides and E. P. Giannelis, *Small,* 2008, **4**, 455.
9. H. T. Li, X. D. He, Z. H. Kang, H. Huang, Y. Liu, J. L. Liu, S. Y. Lian, C. H. A. Tsang, X. B. Yang and S.T. Lee., *Angew. Chem. Int. Ed.,* 2010, **49**, 4430.
10. H. C. Zhang, H. Huang, H. Ming, H. T. Li, L. L. Zhang, Y. Liu and Z. H. Kang, *J. Mater.Chem.,* 2012, **22**, 10501.
11. H. T. Li, R. H. Liu, S. Y. Lian, Y. Liu, H. Huang and Z. H. Kang, *Nanoscale,* 2013, **5**, 3289.
12. D. Y. Pan, L. Guo, J. C. Zhang, C. Xi, Q. Xue, H. Huang, J. H. Li, Z. W. Zhang, W. J. Yu, Z. W. Chen, Z. Li and M. H. Wu, *J. Mater. Chem.,* 2012, **22**, 3314.
13. Y. Xu, M. Wu, Y. Liu, X. Z. Feng, X. B. Yin, X. W. He, and Y. K. Zhang, *Chem. Eur. J.*, 2013, **19**, 2276.
14. R. H. Liu, H. Huang, H. T. Li, Y. Liu, J. Zhong, Y. Y. Li, S. Zhang and Z. H. Kang, *ACS Catal.,* 2014, **4**, 328.
15. S. Y. Xie, R. B. Huang and L. S. Zheng, *J. Chromatogr. A.*, 1999, **864**, 173.
16. S. N. Baker and A. Baker, *J. Angew. Chem.,* 2010, **49**, 6726.
17. G. Luo, H. Yang, M. E. Kose, B. Chen, L. M. Veca and S. Y. Xie, *J. Am. Chem. Soc.,* 2006, **128**, 7756.
18. H. Zhu, X. Wang, Y. Li, Z. Wang, F. Yang and X. Yang, *Chem.Commun.,* 2009, 5118.
19. H. Nie, M. J. Li, Q. S. Li, S. J. Liang, Y. Y. Tan, L. Sheng, W. Shi and S. X.A. Zhang, *Chem. Mater.,* 2014, **26**, 3104.
20. X. Wang, K. Qu, B. Xu, J. Ren and X. Qu, *J. Mater. Chem.,* 2011, **21**, 2445.
21. A. S. Saini, J. Kumar and J. S. Melo, *Analytica Chimica Acta,* 2014 **849**, 50.
22. A. G. Marangoni, Enzyme Kinetics: A Modern Approach, *John Wiley & Sons, Inc.*, 2003.
23. L. Cao, J. Ye, L. Tong and B. Tang, *Chem.-Eur. J*, 2008, **14**, 9633.
24. J. M. Rehm, G. L. Mclendon and P. M. Fauchet, *J. Am. Chem. Soc.,* 1996, **118**, 4490.
25. X. Wang, L. Cao, F. S. Lu, M. J. Meziani, H. T. Li, G. Qi, B. Zhou, B. A. Harruff, F. Kermarrec and Y.P. Sun, *Chem.Commun.,* 2009, 3774.
26. S. M. Henrichs and S. F. Sugai, *Geochim. Cosmochim. Ac.,* 1993, **57**, 823.
27. E. C. Cho, L. Au, Q. Zhang and Y. N. Xia, *Small,* 2010, **6**, 517.
28. S. Chakravarty, V. Dureja, G. Bhattacharyya, S. Maity and S. Bhattacharjee, *Water Res.,* 2002, **36**, 625.
29. M. Del Bubba, C.A. Arias and H. Brix, *Water Res.,* 2003, **37**, 3390.
30. Y. Liu, Z. H. Kang, Z. H. Chen, I. Shafiq, J. A. Zapien, I. Bello, W. J. Zhang and S. T. Lee, *Crystal Growth & Design,* 2009, **9**, 3222.
31. Y. Kubota, H. Yamaguchi, T. Yamada, S. Inagaki, Y. Sugi and T. Tatsumi, *Top. Catal.,* 2010, **53**, 492.

TOC

Fluorescence carbon dots (CDs)/tyrosinase hybrid as fluorescence probe for efficient, fast and sensitive the detection of levodopa.